band 5–35 GHz balun, Microwave Opt Technol Lett 49 (2007), 622–625.
11. M.E. Bialkowski and A.M. Abbosh, Design of a compact UWB out-of-phase power divider, IEEE Microwave Wireless Compon Lett 17 (2007), 289–291.
12. U.-H. Park and J.-S. Lim, A 700 to 2500 MHz microstrip balun using a Wilkinson divider and 3 dB quadrature couplers, Microwave Opt Technol Lett 47 (2005), 333–335.
13. Z. Zhang and S. Xu, A novel balun structure with a conposite right-left-handed transmission line, Microwave Opt Technol Lett 45 (2005), 422–424.
14. A.M. Abbosh and M.E. Bialkowski, An UWB planar out-of-phase power divider employing parallel stripline-microstrip transitions, Microwave Opt Technol Lett 49 (2007), 912–914.
15. Z.-Y. Zhang, Y.-X. Guo, L.C. Ong, and M.Y.W. Chia, A new wideband planar balun on a single-layer PCB, IEEE Microwave Wireless Compon Lett 15 (2005), 416–418.
16. J.-S. Lim, U.-H. Park, Y.-C. Jeong, K.-S. Choi, D. Ahn, S. Oh, and J. J. Koo, 800–5000 MHz ultra-wideband CPW balun, Electron Lett 42 (2006), 35–36.
17. M.-J. Park and B. Lee, Stubbed branch line balun, IEEE Microwave Wireless Compon Lett 17 (2007), 169–171.
18. J.-L. Li, S.-W. Qu, and Q. Xue, Miniaturized branch-line balun with bandwidth enhancement, Electron Lett 43 (2007), 931–932.
19. J.-Y. Ihm and K.-P. Hwang, RF balun embedded in multiplayer organic substrate, Microwave Opt Technol Lett 49 (2007), 473–475.
20. Y.-X. Guo, Z.Y. Zhang, L.C. Ong, and M.Y.W. Chia, A novel LTCC miniaturized dualband balun, IEEE Microwave Wireless Compon Lett 16 (2006), 143–145.
21. D.-H. Kwon, A wideband balun and vertical transition between conductor-backed CPW and parallel-strip transmission line, IEEE Microwave Wireless Compon Lett 16 (2006), 152–154.
22. D.-H. Kwon, Wideband balun and vertical transition between microstrip and parallel-strip transmission line, Microwave Opt Technol Lett 49 (2007), 1530–1532.

MIMO CAPACITY DEPENDENCE ON REALISTIC CROSS-POLARIZATION AND BRANCH POWER RATIOS

David Landon and Cynthia Furse
Department of Electrical and Computer Engineering, University of Utah, Salt Lake City, UT 84112; Corresponding author: cfurse@ece.utah.edu

Received 3 October 2007

ABSTRACT: *The dependence of channel capacity on cross-polarization and the branch power ratio is established over a wide range of both realistic and idealized values. An existing empirical model is adjusted to avoid self-contradictory results for cross-coupled, but uncorrelated energy. Typical ranges are highlighted for realistic channel measurements from the literature, and extreme cases are identified. The value of a peak capacity measure is established and compared with the outage and average capacities.* © 2008 Wiley Periodicals, Inc. Microwave Opt Technol Lett 50: 1384–1388, 2008; Published online in Wiley InterScience (www.interscience.wiley.com). DOI 10.1002/mop.23360

Key words: *MIMO; capacity; channel measurements; channel modeling; cross-coupling; branch power ratio; polarization; normalization*

1. INTRODUCTION

Multi-input multi-output (MIMO) systems continue to receive considerable attention in the literature, because they promise significantly higher capacity than their single-input single-output (SISO) counterparts. Numerous recent studies suggest that polarization diversity is a viable method of boosting channel capacity in MIMO systems [1-7]. This is of particular interest for small handheld communication devices whose small spatial dimensions may prefer the use of dual-polar antennas to spatially separated copolar elements.

But the value of using polarization in MIMO systems has been a matter of debate. Polarization-derived capacity gains vary significantly over various channels and can be quite poor. One cautions, for example, that polarization-based diversity schemes may be penalized by a 3 dB power loss, whereas eight and nine suggest that cross-polarization discrimination levels and polarization-specific path-losses may neutralize expected diversity gains. Other data sets do not confirm these limitations [1-5, 8-10], and these pessimistic voices must be understood in their specific contexts. MIMO capacity measurements depends directly on the channel involved: some channels are well-suited to exploiting polarization, whereas others are not. Channel cross-polarization and imbalanced branch polarization ratios have a demonstrable impact on polarization-based channel capacity. Thus, studies reporting measured data will find varied levels of benefit from polarization-based system design, depending on the nature of their measurement environment.

This poses challenges for the antenna designers who may be frustrated by the large number of measurement campaigns performed in isolated environments. It can be challenging to compare the results because of differing parameters and normalizations or to identify the sensitivity of capacity to particular parameter values. In particular, it can be daunting to address such design questions when a device is intended to be universally deployed over a wide range of environments as is true of commercial cell phones. This work addresses these needs by presenting and adjusting a standard channel model in Section 2, collecting and unifying the presentation of a wide range of polarization parameters to help identify the typical ranges of polarization parameters in Section 3, and resimulating the capacity of each channel and others to indicate dependence of capacity on and sensitivity to these parameters in Section 4. Capacities are reported under an average and outage interpretation and an opportunistic idea of peak capacity is introduced as may be more appropriate to newer cellular systems such as CDMA 2000.

2. CAPACITY AS A FUNCTION OF χ AND BPR

This section presents a framework for modeling polarization-based MIMO and for computing channel capacity. This feeds into a discussion of the range of typical polarization values and from there to representative capacity computations in subsequent sections.

Two primary channel parameters are important to polarization modeling: cross-polarization, χ, and the branch polarization ratio (BPR) or gain imbalance, μ. Cross-polarization is a measure of the degree to which transmitted power of a given polarization is converted to an orthogonal polarization via channel scattering. Gain imbalance expresses a channel's tendency to attenuate one polarization more than another. For example, the disproportionate number of vertical surfaces (walls, windows, etc.) in cities often leads to higher receive power in vertical–vertical polarization subchannels than in horizontal–horizontal polarization subchannels. These values have been characterized in a number of measurements for specific channels, sweeping out ranges of several dB in each parameter in [1, 2, 4, 8-15].

The cross-coupling, χ, has been characterized in a number of measurements for specific channels, sweeping out ranges of sev-

eral dB in Ref. [1, 2, 4, and 8-15]. A general dual-polarized channel matrix model can be used to express the way cross coupling characterizes channel behavior. A channel matrix, H, is defined for a narrowband channel, to describe the relationship between the transmit voltages, x, present at N_T transmit antennas and the receive voltages, y, present at N_R receive antennas as

$$\underbrace{y}_{N_T \times 1} = \underbrace{H}_{N_T \times N_R} \underbrace{x}_{N_R \times 1}. \tag{1}$$

The elements of H may represent purely copolarized elements or cross-coupling may be included in a partitioned form reflecting the receive and transmit polarizations of corresponding antennas via the subscripts V or H, representing vertical, and horizontal polarizations, respectively [16]:

$$y = \begin{bmatrix} H_{VV} & H_{VH} \\ H_{HV} & H_{HH} \end{bmatrix} x. \tag{2}$$

To include both the effects of cross-coupling and BPR, the authors of [16] construct a root power covariance correlation matrix $\Gamma = R \times P$ *where the operators* $\sqrt{\cdot}$ *and* $\times$ *are element-wise, and* R and P are the block correlation and power covariance matrices as defined in Ref. [16]. Samples of H are then modeled with this Γ-specified distribution as $H = U_\Gamma \Lambda_\Gamma^{1/2} H_{iid}$ via the singular value decomposition $U_\Gamma \Lambda_\Gamma V_\Gamma^H = \Gamma$ and an uncorrelated version of H with independent, identically complex-normal-distributed (iid) elements. Now by virtue of this construction, $E\{HH^H\} = \Gamma$. Cross-coupled energy can indeed be correlated because of poor antenna polarization discrimination or poor isolation, or even from channel effects such as the atmospheric Faraday rotation experienced by satellite channels. In such cases, simulation of H via Γ is the correct approach.

However, when cross-coupled energy is uncorrelated through scattering or other mechanisms, this approach is inaccurate. H then cannot depend on P through the singular value decomposition given above. The issue is not problematic for $\chi \approx 0$, leaving the results of Ref. [16] essentially unchanged. However, the preceding model only allows $\chi \approx 1$ if energy in each polarization is highly correlated. To admit power imbalances without correlation as will be modeled in this work, one must use a singular value decomposition of just $\sqrt{R}$ and the element-wise multiplication

$$H = P \times U_R \Lambda_R^{1/2} H_{iid}. \tag{3}$$

This approach is similar to the model in Ref. [17] (which ignores BPR and uses a trivial correlation matrix), still agrees with the data of 16, and avoids the limitation of the former model.

Considerable insight can be drawn from the simplest dual-polar model in which H is 2×2 and represents a single vertical- and a single horizontal-polarized element on each side of the link. In this case, the partitioned matrix, R, consists of four 1×1 identity matrices as does its element-wise square root, leaving $\Gamma = P$. For this 2×2 case, one could reasonably construct P as:

$$P = \begin{bmatrix} 1 & \chi_{RT}\mu_T \\ \chi_{TR}\mu_R & \mu_R\mu_T \end{bmatrix}, \tag{4}$$

where μ_R and μ_T are the receive and transmit BPRs, respectively and χ_{RT} and χ_{TR} represent the transmit-receive and receive-transmit cross-coupling terms, respectively. Although the ability to separate transmit and receive BPR values is present in the model given in Ref. [16], most measurement campaigns offer less detail about the source of various power imbalances, defining simply $\dot{\iota} = H_{22}{}^2/H_{11}{}^2$, $\div_{RT} = H_{12}{}^2/H_{11}{}^2$, and $\div_{TR} = H_{21}{}^2/H_{22}{}^2$. This leads to a simpler form used to summarize the measurements in Table 1, where χ_{RT} and χ_{TR} actually subsume BPR losses as well as cross-coupling:

$$P = \begin{bmatrix} 1 & \chi_{RT} \\ \chi_{TR} & \mu \end{bmatrix}. \tag{5}$$

Channel capacity may be computed from an appropriately normalized form of the channel matrix, H_{norm}, depending on the level of channel state information available at the transmitter. In the absence of such information, the transmitter assigns equal power to each transmitter. Then equal power capacity is computed as [18] $C_{EP} = \log_2 \left| I + (SNR/N_T) H_{norm} H_{norm}^H \right|$, where SNR is the signal to noise ratio, $|A|$ is the determinant of A, and A^H is the conjugate transpose of A. When complete knowledge of the channel is available, optimal power allocation is performed using the water filling algorithm [13, 19, 20], and generally surpasses C_{EP}. This work investigates the dependence of capacity on normalization for varying cross-polarization levels.

Among authors attempting to accommodate dual-polar signaling, H is most often normalized as $H_{norm} = H/K_{copolar}$, where $K_{copolar}$ is computed from the Frobenius norm of the all-vertical subblock of H with dimensions $N \times M$ as Ref. [21]:

$$K_{copolar} = \sqrt{\frac{E\{\|H_{VV}\|_F^2\}}{NM}}. \tag{6}$$

However, to avoid artificially inflating transmit power in highly cross-coupled channels, it is best extended to account for cross-coupling as [22]:

$$K_{extended} = \sqrt{\frac{(1+\chi) E\{\|H_{VV}\|_F^2\}}{NM}}. \tag{7}$$

3. REALISTIC CROSS-COUPLING AND BRANCH-POLARIZATION-RATIO VALUES

Many researchers report values of χ and μ or at least one of the two parameters measured in a variety of channels, and this section discusses the range of values found in the literature and their significance on channel capacity. Because values may be reported in a manner inconsistent from publication to publication (i.e., as positive or negative dB values, or as squared or non-squared values, etc.), it is important to list the parameters used in this work in a single, consistent fashion. Several representative channels are mentioned in Table 1, which represents a subset of the data provided in the cited works. Table 1 represents the widest range of χ- and μ-values found by the authors in the literature. Design engineers may particularly benefit from this table, as it helps sweep out likely ranges of χ and μ for realistic channels and predicts capacities for channels both similar and dissimilar to these examples.

The final columns of Table 1 also provide various capacity estimates representing 5000 realizations of H computed using (3), (4), and (7) for each pair of μ and χ, assuming $\mu_T = 1$, $\mu = \mu_R$, and $\chi_{RT} = \chi_{TR}$. C_E, the ergodic or average capacity is an ensemble average capacity over these 5000 realizations, whereas outage capacity, $C_{0.1}$ is the capacity exceeded all but 10% of the time and peak capacity is exceeded just 5% of the time over the ensemble of simulated channel matrices. The relevance of each statistic and each constraint on μ and χ is explored in Section 4.

A number of interesting points are evident in the measured channels collected in Table 1. Cross-polarization values range

TABLE 1 A Compilation of Measured Channel Parameters and Capacities

M(dB)	χ_{HV} (dB)	χ_{VH} (dB)	Source	Notes	$C_{0.1}$ percent above C_{SISO}[a]	E{C} percent above C_{SISO}[a]	$C_{0.95}$ percent above C_{SISO}[a]
Indoor LOS (hallway, etc.)							
..	−15	−15	Kyritsi et al. [2]	Hallway	3	50	98
..	−6.8	−6.8	Wallace et al. [3]	Hallway	6	45	93
Indoor NLOS							
..	0	0	Kyritsi et al.[2]	−15 dB + LOS power	9	43	83
3.2[b]	2.2	−7.0	McGladdery and Stapleton [8]	High angle reflections	−10	18	59
..	−2.5	−2.5	Cox et al. [10]	Homes, buildings	8	44	85
..	−4.5	−4.6	Ho and Rappaport [14]		7	45	89
Outdoor LOS							
−6– −7	−13	−13	Oestges et al. [12][c]	[10, Section 2. C.1]	−20	19	64
..	..	−12	Vaughn [11]		4	49	97
..	..	−7	Vaughn [11]	Urban	6	44	93
..	−3	−3	Weitzen and Wallace [4]	χ varies from −3 to −10	8	44	85
	−10	−10	Weitzen and Wallace [4]	(Labeled Weitzen 10)	4	48	96
Outdoor NLOS							
±3	−6	−6	Lee and Yeh [1]	Car-mounted elements driven along NJ streets	−4	32	77
..	−2	−2	Weitzen and Wallace [4]	Distant *and* LOS	9	43	84
..	−3.5	−3.5	Cox et al. [10]	Outside homes and large buildings	8	44	86
−3	−3	−3	Kovács et al. [9]	1.9 GHz, forest	−2	31	74
−3	−10	−10	Kovács et al. [9]	χ varies from -3 to -10	−7	34	80
−5	0	0	Kovács et al. [9]	0.4 GHz, typical hilly-terrain forest	−8	23	60
−5	−2.5	−2.5	Kovács et al. [9]	0.4 GHz, typical flat-terrain forest	−9	24	63

A pair of dots (..) indicates a parameter not reported by the source.

[a] C_{SISO} and $C_{0.1}$, E{C} and $C_{0.95}$ are explained in Section 2.

[b] McGladdery's measurement seems rather unlike the others, and reasons for this difference are not obvious.

[c] Oestges' results are actually the result of sophisticated single bounce ray-tracing simulations. They offer the most detailed distributions for χ and μ, but may be somewhat idealized. As a result, conclusions drawn from this channel may be more idealized than is common in real channels.

over roughly $0 > \chi > -15$ dB, with an anomalous (positive) value reported by McGladdery and Stapleton[8]. His measurement suggests that horizontal polarizations are almost entirely preserved in his channel, and virtually all energy of vertical polarization cross-couples into horizontal polarization and adds to this power, an unusual result in most channels. Cross-polarization values close to 0 dB are typical in nonline-of-sight channels (NLOS), and more strongly negative values are typical of line-of-sight channels (LOS). This distinction proves more important than whether a user is indoors or outdoors. Readers are cautioned against assuming that LOS channels such as the hallway measurement campaigns by Wallace and Kyritsi are representative of NLOS indoor channels such as those involving transmissions between most rooms in a building. Finally, χ_{HV} and χ_{VH} are generally very nearly equal. Even in Ref. 25, where the reader is explicitly warned that this is not universally true, the power difference is less than 2% and hardly offers a contradiction to this rule of thumb.

Branch polarization ratios are grouped closer to zero with typical values of $+3.2 > \mu > -7$ dB. The fact that μ is less commonly reported than χ suggests that it is often not apparent in data sets, that is, it may be rather close to 0 dB in many channels as is stated in Ref. [23]. This is to be expected in LOS channels or whenever vertical and horizontal scattering surfaces are roughly evenly distributed in a channel. Nonzero values are common indoors, in cities, or in wooded areas, which tend to contain disproportionate numbers of vertical surfaces. In fact, ratios near −3 dB also seem likely as they are most commonly reported if any ratio is reported at all. In Ref. [16], a BPR range of [0 dB, 30 dB] is considered, but only in simulation with measured values of only −1.6 dB and −7.5 dB. The next section simulates channel capacities over a range of χ and BPR values as a baseline for what might be achievable with a practical antenna design in realistic channels.

4. CAPACITY SIMULATIONS

Table 1 summarizes and Figure 1 compares the average or ergodic capacity, C_E, computed via waterfilling over 5000 channel realizations for a link with colocated, dual-polarized antennas (vertical-horizontal [VH]) at each end. H is computed using (3) and (4) and normalized according to (7). χ_{HV} and χ_{VH} are chosen to be equal as is commonly the case and vary as χ in the abscissa of the plot. μ_R is also varied as labeled next to each contour and μ_T is set to 1. This represents the asymmetric case of an elevated base station transmitting to a mobile surrounded by clutter and polarization selective surfaces. Capacities are reported as a percentage improvement over the capacity available in a SISO channel, where SISO $C_E = \log_2(1 + 20\text{dB}) = \log_2(1 + 100) = 6.66$ bits/use. Thus, gains are reported as $(C_{simulated} - C_{SISO}) \times 100\%/C_{SISO}$ both in these plots and in all other plots in this work.

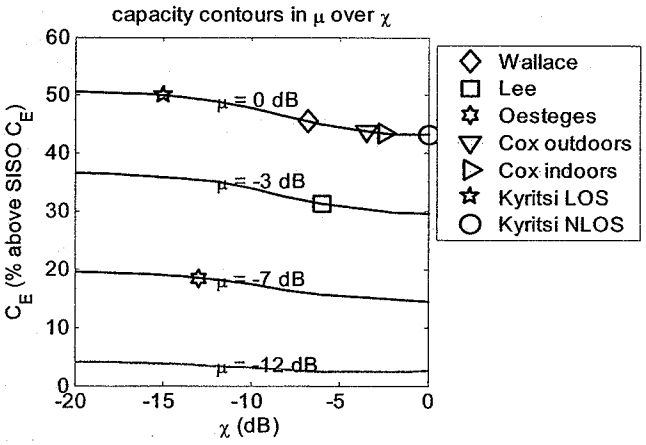

Figure 1 Average capacity, C_E, as a function of χ and μ. Named channels from Table 1 are included as indicated. As long as μ is near 0 dB, capacity is nearly 1.5 times that offered on average by a SISO channel. [Color figure can be viewed in the online issue, which is available at www.interscience.wiley.com]

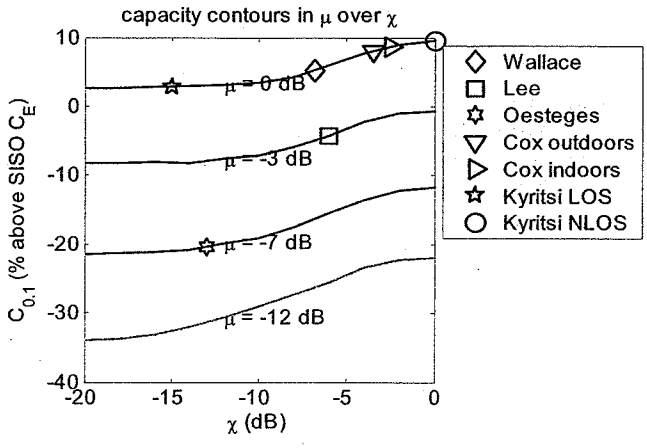

Figure 3 Outage capacity, $C_{0.1}$, as a function of χ and μ. Named channels from Table 1 are included as indicated. With these penalties relative to SISO channel, one may consider using diversity branches to mitigate fades rather than to boost capacity. [Color figure can be viewed in the online issue, which is available at www.interscience.wiley.com]

Sweeping out each of the (χ, μ) coordinates representing each of the channels reported in Table 1 (and numerous additional χ, μ pairs) allows for the construction of a three-dimensional surface relating capacity to various channel descriptions. Figures 1–3 plot this functional as a contour plot over fixed μ-contours, varying χ-values along the horizontal axis and reporting capacity along the vertical axis. Each subplot of Figure 2 represents a different interpretation of capacity. In all cases, capacity is reported as the percent of capacity gain relation with C_{SISO} as described for Figure 1. When χ is extremely small and μ near one, the channel forms two uncoupled subchannels of equal quality. This gives an idealized uncoupled capacity of $C = 2\cdot\log_2(1 + 100/2) = 11.34$ bits/use or 70% over $C_{SISO} = 6.67$ bits/use. As one should expect, because of the small-scale fading fluctuations of Rayleigh-fading channels modeled by the complex-normal distributed elements of H_{iid}-the peak capacity reported in Figure 2 exceeds this level, whereas the average capacity falls short of this idealized average level as shown in Figure 1.

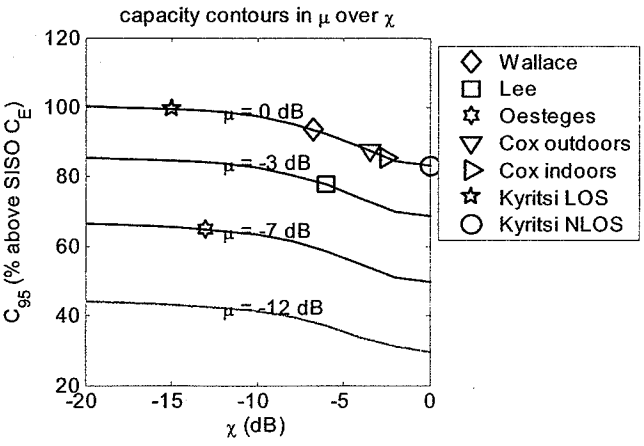

Figure 2 Peak capacity, C_{95}, as a function of χ and μ. Named channels from Table 1 are included as indicated. As long as μ is near 0 dB in such an opportunistic scenario, capacity is nearly double that offered on average by a SISO channel. [Color figure can be viewed in the online issue, which is available at www.interscience.wiley.com]

The average capacity, C_E, plot of Figure 1, shows that many realistic channels (i.e., those of Table 1 and listed in the legend of the plot) offer a polarization-derived capacity benefit of 20–50% over C_{SISO}. Outage capacity-a measure of link reliability-$C_{0.1}$, or the capacity exceeded 90% of the time, is given in Figure 3 and can be estimated from the largest capacity among the smallest 10% of the sorted ensemble of simulated waterfilling capacities. This statistic is also commonly reported and may be more appropriate whenever link margins are low and the risk of irreparably corrupting data bits is nonnegligible. Finally, the peak capacity achieved 5% of the time, $C_{0.95}$, presents itself as a measure of particular value in opportunistic, multiuser systems and is given in Figure 2. This measure can be estimated from the smallest capacity among the largest 5% of the capacities in an ensemble of simulated capacities. In opportunistic communication scenarios, such as that defined by CDMA 2000, users are assigned time slices when they experience favorable environmental conditions [24]. In such schemes, each user actually sees a channel the capacity of which can actually exceed the idealized average uncoupled channel capacity because of random fluctuations in the channel around its mean signal strength.

Deciding which measure of capacity is most appropriate is a system design question. In any case, the outage and peak capacity measures offer useful upper and lower bounds on expected link quality. As evident in Figure 3, outage capacity gains vary considerably over realistic channels. Those channels reported in Table 1 offer outage gains of as much as 10% for a channel with negligible branch polarization ratio to as little as 20% less than the *average* capacity of a SISO channel for a channel with $\mu = -7$ dB. Much more pessimistic results would be evident for an outage capacity defined in terms of the capacity exceeded 99% of the time as is also considered in the literature. When such a stringent performance measure is used, it is likely wise to use the multiantenna system for diversity combining to reduce the impact of fades rather than for multiplexing intended to increase capacity. Figure 2 suggests that peak capacity $C_{0.95}$ is somewhat less sensitive to variations in χ and μ over the range of channels reported in Table 1. Capacity gains drop from a range of 80–100% to 50–65% as μ drops from 0 dB to -7 dB as a consequence of the reduced

power available at the receiver. A similar drop in capacity ranges is evident as the channel cross-polarization increases from -15 dB to 0 dB because the channel matrix is more often rank-deficient.

For a system designer, it may be less important to know the capacity gain likely for a given input parameter set, (X_0, μ_0), than to know how capacity varies over an expected range of input parameters, $\chi_0 < \chi < \chi_1$, and $\mu_0 < \mu < \mu_1$. Figures 1–3 prove useful here as well. In a NLOS channel such as the indoor channel reported by Cox 12, a 3 dB reduction in χ moves the relative outage capacity gain over SISO C_E from 9% to 5%, whereas a 3 dB reduction in μ drops the outage capacity to 2% below the averave SISO capacity. Though the capacity is sensitive to variations in both μ and χ, these channels appear most sensitive to μ the value of which largely dictates the quality of the secondary channel available for multiplexing.

5. CONCLUSIONS

Although idealized extremes bound the ergodic capacity gain over C_{SISO} by 0%–70%, realistic channels appear to rarely reach either extreme. Instead, ergodic capacity gains tend to range from 20% to 50% as a function of realistic cross-coupling ($0 > \chi > -15$ dB) and branch power ratios ($+3 > \mu > -7$ dB). Other definitions of capacity include outage capacity and peak capacity. Each leads to higher or lower expected gains, respectively, for the same channel assumptions. When outage capacity is measured typical gains are as high as 10% over the average SISO channel capacity for a generous outage capacity definition, $C_{0.1}$. In contrast, opportunistic scheduling better characterized by peak capacity makes polarization a consistent source of gains exceeding 65% above C_{SISO} for virtually all real channels. Capacity is very sensitive to μ and relatively sensitive to χ when it is near unity.

ACKNOWLEDGMENTS

This project was supported in part by the National Science Foundation (ECS-0524720000).

REFERENCES

1. W.C.-Y. Lee and Y.S. Yeh, Polarization diversity system for mobile radio, IEEE Trans Commun 20 (1972), 912–923.
2. P. Kyritsi, D.C. Cox, R.A. Valenzuela, and P.W. Wolniansky, Effect of antenna polarization on the capacity of a multiple element system in an indoor environment, IEEE J Select Areas Commun 20 (2002), 1227–1239.
3. J.W. Wallace, M.A. Jensen, A.L. Swindlehurst, and B.D. Jeffs, Experimental characterization of the MIMO wireless channel: Data acquisition and analysis, IEEE Trans Wireless Commun 2 (2003), 335–343.
4. J. Weitzen and M. Wallace, Analysis of diversity perfomance of space diversity and cross polarization for PCS base stations, IEEE Personal Indoor Mobile Radio Commun 1 (1998) 293–297.
5. T.B. Sørensen, A.Ø. Nielsen, P.E. Mogensen, M. Tolstrup, K. Steffensen, and F. Bajers, Performance of two-branch polarization antenna diversity in an operational GSM network, In the 48th Vehicle Technology Conference, 1998, p. 741–746.
6. M.J. Fakhereddin and K.R. Dandekar, Combined effect of polarization diversity and mutual coupling on MIMO capacity, IEEE Antennas Prop Soc Int Symp 2 (2003), 495–498.
7. R.U. Nabar, H. Bölcskei, V. Erceg, D. Gesbert, and A.J. Paulraj, Performance of multiantenna signaling techniques in the presence of polarization diversity, IEEE Trans Signal Proces 50 (2002), 2553–2562.
8. W.A. McGladdery and S. Stapleton, Investigation of polarization effects in indoor radio propagation, In the IEEE International Conference on Selected Topics in Wireless Communications, 1992, pp. 53–56.
9. I. Z. Kovács, P. C. Eggers, K. Olesen, Characterization of cross polarization discrimination in forest environments, In 52nd Vehicle Technology Conference, 2, 2000, pp. 725–731.
10. D. Cox, R. Murray, H. Arnold, A. Norris, and M. Wazowicz, Cross-polarization coupling measured for 800 MHz radio transmission in and around houses and large buildings, IEEE Trans Antennas Propag 34 (1986), 83–87.
11. R.G. Vaughan, Polarization diversity in mobile communications, IEEE Trans Vehicular Tech 39 (1990), 177–186.
12. C. Oestges, V. Erceg, and A.J. Paulraj, Propagation modeling of MIMO multipolarized fixed wireless channels, IEEE Trans. Vehicular Technol 53 (2004), 644–654.
13. J.W. Wallace, Modeling electromagnetic wave propagation in electrically large structures. Brigham Young University. [Online]. Available at: http://www.ycomm.org., 2002.
14. C.M.P. Ho and T.S. Rappaport, Effects of antenna polarization and beam pattern on multipath delay spread and path loss in indoor obstructed wireless channels, Proc. Universal Personal Communications, 1992, pp. 04.02.1-5.
15. B. Fong, P.B. Rapajic, A.C.M. Fong, and G.Y. Hong, Polarization of received signals for wideband wireless communications in a heavy rainfall region, IEEE Commun Lett 7 (2003), 13–14.
16. J.P. Kermoal, L. Schumacher, F. Frederiksen, and P.E. Mogensen, Polarization diversity in MIMO radio channels: experimental validation of a stochastic model and performance assessment, In the 56th Vehicle Technology Conference, 2, 2002, pp. 941–945.
17. J.W. Wallace and M.A. Jensen, Modeling the indoor MIMO wireless channel, IEEE Trans Antennas Propag 50 (2002), 591–599.
18. M.A. Jensen and J. Wallace, A Review of antennas and propagation for MIMO wireless communications, IEEE Trans Antennas Propag 52 (2004), 2810–2824.
19. G.G. Raleigh and J.M. Cioffi, Spatio-temporal coding for wireless communication, IEEE Trans Commun 46 (1998), 357–366.
20. D. Tse and P. Viswanath, Fundamentals of Wireless Communication, Cambridge University Press, 2004.
21. V.R. Anreddy and M.A. Ingram, Capacity of measured Ricean and Rayleigh indoor MIMO channels at 2.4 GHz with polarization and spatial diversity, IEEE Wireless Com Networking Conf 2 (2006), 946–951.
22. D. Landon, C. Furse, Inclusion of Cross-coupling in MIMO Capacity Normalization, submitted to IEEE Transactions on Antennas and Propagation.
23. H. Özcelik and C. Oestges, Some remarkable properties of diagonally correlated MIMO channels, IEEE Trans Veh Tech 54 (2005), 2143–2145.
24. P. Viswanath, D. Tse, and R. Laroia, Opportunistic beamforming using dumb antennas, IEEE Trans Inform Theory 48 (2002), 1277–1294.